Modeling an ultra-rare epilepsy variant in wildtype mice with in utero prime editing

Colin D. Robertson[1], Patrick Davis[2], Ryan R. Richardson[1], Philip H. Iffland II[3], Daiana C. O. Vieira[4], Marilyn Steyert[1]†, Paige N. McKeon[1], Andrea J. Romanowski[1], Garrett Crutcher[1], Eldin Jašarević[1]†, Steffen B. E. Wolff[1], Brian N. Mathur[1], Peter B. Crino[3], Tracy L. Bale[1]†, Ivy E. Dick[4], Alexandros Poulopoulos[1]*

[1]Department of Pharmacology and UM-MIND, University of Maryland School of Medicine, Baltimore, MD, USA

[2]Department of Neurology, Boston Children's Hospital, Harvard Medical School, Boston, MA, USA

[3]Department of Neurology, and UM-MIND, University of Maryland School of Medicine, Baltimore, MD, USA

[4]Department of Physiology and UM-MIND, University of Maryland School of Medicine, Baltimore, MD, USA

*Corresponding author. Email: apoulopoulos@som.umaryland.edu

†Current affiliations: MS: Department of Neurological Surgery, University of California San Francisco; EJ: Department Computational and Systems Biology, Department of Obstetrics, Gynecology and Reproductive Sciences, University of Pittsburgh School of Medicine; TB: Department of Psychiatry, University of Colorado School of Medicine.

Abstract: Generating animal models for individual patients within clinically relevant time frames holds the potential to revolutionize personalized medicine for rare genetic epilepsies. By incorporating patient-specific genomic variants into model animals, capable of replicating elements of the patient's clinical manifestations, a range of applications would be enabled: from preclinical platforms for rare disease drug screening, to bedside surrogates for tailoring pharmacotherapy without subjecting the patient to excessive trial medications. Here, we present the conceptual framework and proof-of-principle modeling of an individual epilepsy patient with an ultra-rare variant of the NMDA receptor subunit GRIN2A. Using in utero prime editing in the embryonic brain of wildtype mice, our approach demonstrated high editing precision and induced frequent, spontaneous seizures in prime editor-treated mice, reflecting key features of the patient's clinical presentation. Leveraging the speed and versatility of this approach, we introduce PegAssist, a generalizable 7-week workflow for bedside-to-bench modeling of patients using in utero prime editing. These individualized animal models can allow for widely-accessible personalized medicine for rare neurological conditions, as well as accelerate the drug development pipeline by providing an efficient and versatile preclinical platform for screening compounds against ultra-rare genetic diseases.

Introduction

Genetic epilepsies exhibit significant etiological heterogeneity, with nearly 1000 associated gene variants identified and corresponding diversity in clinical manifestations (*1*, *2*). While prevalent in aggregate, genetic epilepsies largely comprise ultra-rare variants (*3*) for which treatment options are limited due to challenges in assembling large study trial cohorts.

More than half of all epilepsy patients require multiple trials of medications and approximately 30% of patients nonetheless remain resistant to pharmacotherapy (*4*). Even in patients with a known genetic cause of epilepsy, reliable prediction of therapeutic or deleterious response to medication trials remains elusive (*2*). In this space of inadequately treated ultra-rare epilepsies, a platform to identify patient-specific efficacies through existing anti-epileptics or the off-label use of compounds approved for human use would offer a path toward systematizing treatment selection in a manner that would otherwise not be clinically feasible.

For personalized medicine approaches to be applicable in a clinical setting, the technology for producing personalized model animals needs to be i) rapid, applicable in clinically relevant time scales, ii) versatile, applicable to a range of patients with distinct genetic variants, and iii) validatable, able to recapitulate identifiable features of the individual's clinical presentation that are measurable against therapeutic interventions.

We present PegAssist, an experimental approach which demonstrates these features by leveraging developments in somatic cell genome editing and new precision editors (*5–7*) in a workflow applicable within weeks (Fig. 1). We used prime editing in utero to genomically introduce an epilepsy patient point-variant into the brain of individual wildtype mice. The PegAssist platform produced individualized animal models that displayed frequent, spontaneous seizures reproducing several core characteristics of the clinical presentation of the patient.

Prime editing 3b demonstrates high editing precision

We began by screening available and engineered high-performance genome editors (*8*, *9*) for high on-target precision, assessed by the rate of intended over unintended edits on the genome . Precision is the key limiting parameter for in vivo somatic cell genome editing, in order to introduce the intended edit in the body without accumulating unintended loss-of-function edits (*6*). We assessed on-target precision by point editing a genomically-encoded Blue Fluorescent Protein (BFP) gene with agents to introduce the substitution H62Y, which corresponds to the sequence for Green Fluorescent Protein (GFP). Precise editing would convert BFP to GFP, while on-target loss-of-function errors (e.g.: indels) would result in loss of fluorescence (Fig. 2A and fig. S1).

With this strategy we quantified editing precision of homology-directed recombination (HDR) and homology-mediated end-joining (HMEJ) strategies with Cas9 and Cas9-CtIP (*8*), as well as of reverse transcriptase-mediated editing with Prime Editor (PE) and PE fused to hRad51 in both PE2 and PE3b strategies (*9*) (fig. S1b-c). This screen demonstrated exceptionally high precision of point editing with the PE3b strategy, yielding the correct edit over 5-fold more frequently than the aggregate of all other edits (Fig. 2B-C).

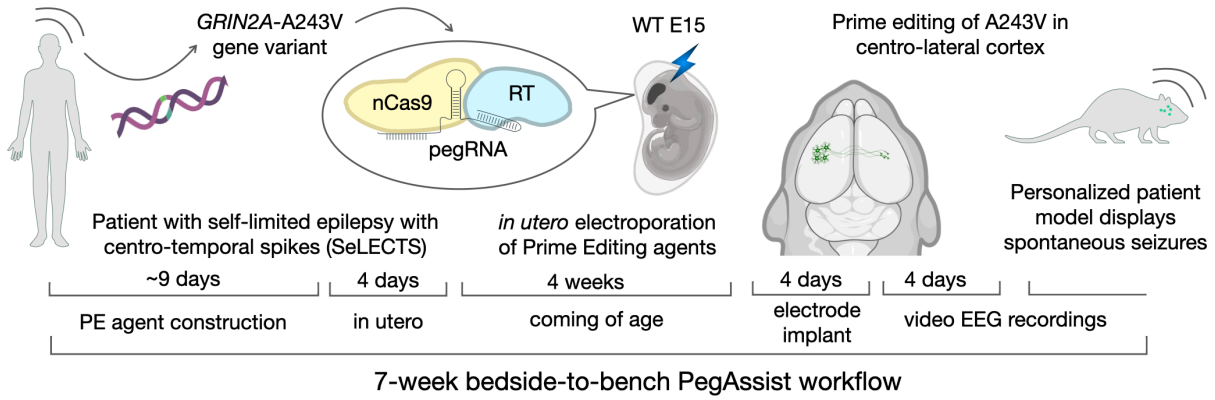

Fig. 1. "PegAssist" personalized animal model workflow. Schema depicting the 7-week PegAssist workflow for personalized animal models, beginning from variant identification, and including genome editing agent construction, in utero delivery, and baseline analysis of personalized animal models.

PE is a hybrid ribonucleoprotein consisting of a protein fusion of Cas9 nickase (nCas9) and reverse transcriptase (RT), in complex with a hybrid pegRNA consisting of a "spacer" sequence for nCas9 targeting, a "primer binding sequence" that hybridizes with nicked genomic DNA, and template sequence for RT to encode the edit. To employ the PE3b strategy, an independent gRNA with no RT component directs PE to nick the complementary strand to encourage productive pegRNA-mediated editing (Fig. 2D). To facilitate the design and production of PE agents, we created pegassist.app, a python-based webtool and plasmid set offered through Addgene (fig. S2 and Methods). This webtool may be used in tandem with other pegRNA design tools to optimize editing agent production (*11*, *12*).

In utero prime editing of GRIN2A variant from epilepsy patient

The exceptional performance of PE3b prompted us to explore its use directly in vivo to model an individual patient variant in wildtype mice. We selected to model a patient with self-limited epilepsy with centrotemporal spikes (SeLECTS) reported with an ultra-rare missense variant, A243V, in the *GRIN2A* gene, encoding the 2A subunit of the N-methyl-D-aspartate (NMDA) type glutamate receptor (*13*). GRIN genes are hotspot loci with hundreds of ultra-rare loss- and gain-of-function variants identified to cause conditions collectively termed GRINopathies that commonly present with seizures that range in severity and manifestation (*14*). Importantly, *Grin2a* knockout mice do not have spontaneous seizures (*15*). The considerable genotypic and phenotypic diversity among patients with GRIN2-related disorders (*16*) further highlights the importance of modeling patient-specific variants in animal models (*3*, *17*).

We constructed PE3b agents to edit the A243V patient variant into the *Grin2a* locus of the mouse using pegassist.app (Fig. 2D and fig. S2). PE and fluorescent reporter plasmids were injected into the lateral telencephalic ventricle of E15 mouse embryos and targeted by in utero electroporation to upper layer pyramidal neurons in centrolateral cortex (Fig. 2E), broadly analogous to the area of centrotemporal cortex, where epileptiform activity is detected in patients with SeLECTS.

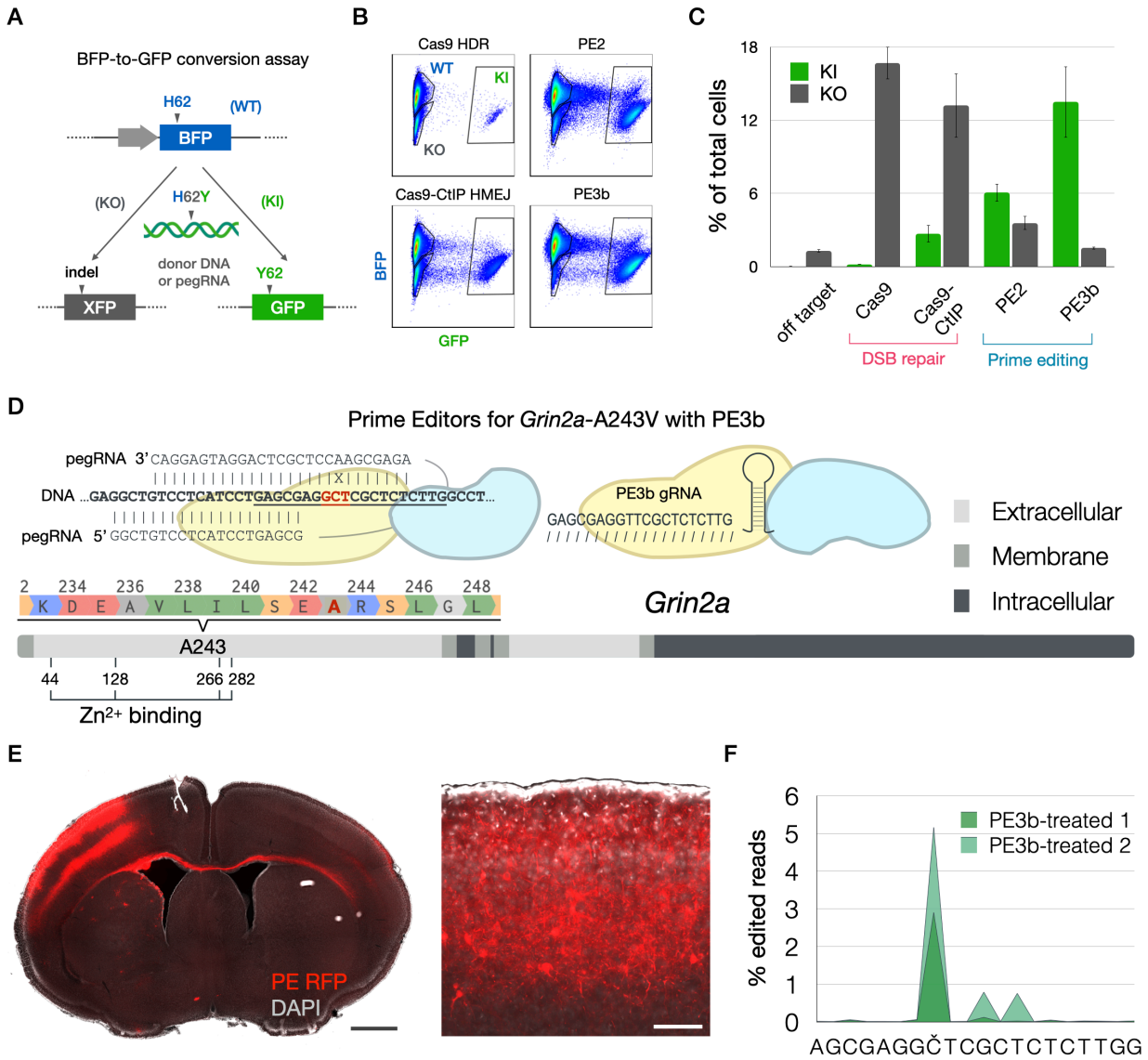

Fig. 2. Genomic insertion of epilepsy patient variant of *GRIN2A* with in utero Prime editing. (**A**) Schema of BFP-to-GFP conversion assay to assess editor precision. (**B**) FACS plots and (**C**) quantification of blue unedited (WT), green correctly edited (knock-in; KI), and dark incorrectly edited (knock-out; KO) HEK cells after treatment with double-strand-break (DSB) repair editors Cas9 (with homology directed recombination [HDR] template) and Cas9-CtIP (with homology-mediated end-joining [HMEJ] template), and prime editing strategies PE2 and PE3b. PE3b outperforms other editing strategies through both higher KI rates and lower KO rates. (**D**) Alignment and schema of the WT *Grin2A* target sequence with the pegRNA and PE3b gRNA used to introduce edit A243V. Underlined is the sequence targeted by the PE3b gRNA. In red is the codon for A243. X shows the mismatch between target sequence and pegRNA RT template that introduces the A243V edit. The grey scale bar represents GRIN2A protein primary sequence with cellular topology as indicated in the key. Edited residue A243 and critical residues for Zn^{2+}-binding are indicated. (**E**) Coronal section of DAPI-stained (grey) brain electroporated with PE and fluorescent marker (red) in centro-lateral cortex. Magnified inset shows electroporated upper-layer pyramidal neurons expressing PE. Scale bar = 1 mm, inset 100 µm. (**F**) Sequencing plot from fluorescence-sorted neurons from PE3b-treated mice showing the percentage of sequencing reads that deviated from the reference sequence around the genomic target sequence encoding A243. The intended nucleotide to be edited is marked as Č. Editing predominantly occurs on the intended base.

Animals electroporated in utero with either PE or control plasmids came to term and were allowed to reach adulthood in their home cage.

We directly assessed editing performance in vivo in two PE3b-treated mice by dissociating and sorting fluorescent cells from the electroporated target area of cortex. RNA sequenced from sorted cells showed moderate editing efficiency, but high editing precision: the A243V edit was present in ~5% of reads, while less than 1% of reads displayed any on-target errors (Fig. 2F and fig. S3).

This performance is similar to the >5-fold prevalence of precise edits we observed for PE3b editing in vitro (Fig. 2C), and corresponds to orders-of-magnitude higher precision than other knockin approaches we previously tested (*10*). Further, this likely is an underestimate of editing precision, since substitutions appear in sequencing reads as technical artifacts, e.g. due to RT or PCR amplification errors during library preparation (*18*), which we did not attempt to discriminate from true editing errors. Importantly, the rate of insertion / deletion events (indels) was minimal (<0.001%), indicating that loss-of-function effects are not a significant editing outcome.

We additionally confirmed using electrophysiology that PE-electroporated neurons do not display *Grin2a* loss of function. NMDA currents of PE-electroporated neurons in culture were largely normal, unlike Cas9-electroporated *Grin2a* knockout neurons, which displayed pronounced reduction in Zn^{2+} blockade of NMDA currents (fig. S4), as expected by *Grin2a* loss of function (*19*). Using exogenous expression in HEK cells, we corroborated that the *Grin2a*-A243V variant does not measurably alter gating effects of Zn^{2+}, in contrast to a previous report in oocytes (*13*). Taken together, these data show that our in utero PE3b strategy successfully incorporated the patient variant into the *Grin2a* locus in vivo, without detectable loss of function.

In utero prime edited "PegAssist" mice carrying patient variant display spontaneous seizures

Having confirmed in vivo editing in a subset of neurons in centrolateral cortex of wildtype mice, we proceeded to monitor 7 PE-electroporated "PegAssist" (PA) and 6 control-electroporated (CT) mice using video-EEG for 96 hours to determine whether animals present any pathological features associated with SeLECTS. 3 of 7 PA animals displayed spontaneous seizures with behavioral and electrographic features similar to those seen in SeLECTS patients (Fig. 2A, fig. S5, and movies S1-4) (*20*, *21*).

Two of the PA animals (PA2 and PA5) showed frequent, spontaneous motor seizures associated with asymmetric tonic posturing with hemiclonic movements (movies S1-4). Focal motor and secondarily generalized seizures are both typical of patients with SeLECTs. As shown in the representative traces in Fig. 3A, events in PA2 and PA5 were electrographically characterized by sharply contoured, evolving spike-and-wave discharges in the ~5 Hz range. As evident in example spectrograms and averaged traces (Fig. 3B and fig. S5), these events have discrete onset and termination with consistent frequencies. This event type represented the majority of observed seizures. A second seizure type was observed in animal PA6, a single generalized electrographic seizure without a motor component occurring during sleep (Fig. 3A, PA6).

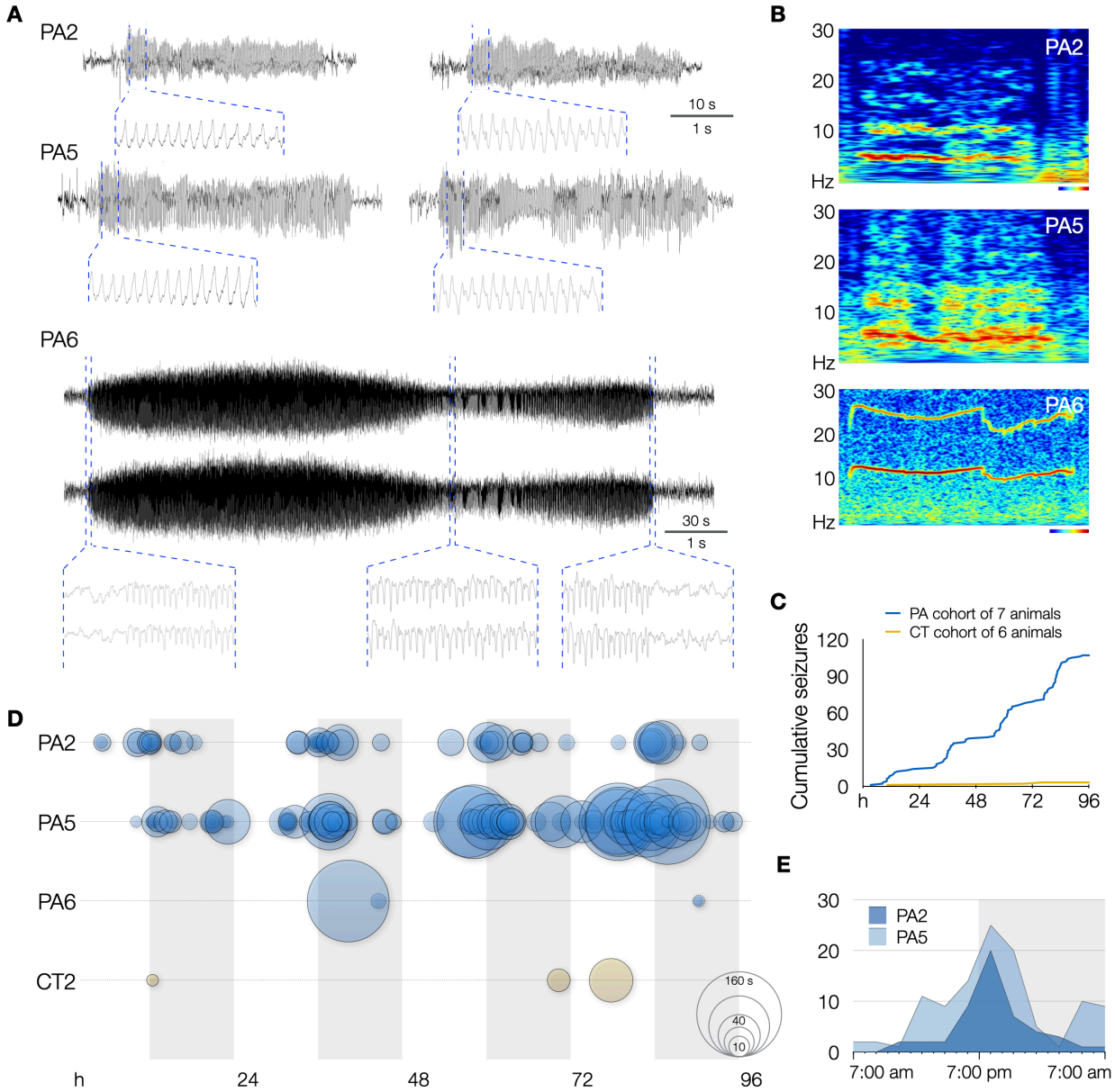

Fig. 3. PegAssist *Grin2a*-A243V mice develop frequent spontaneous seizures. (**A**) Representative EEG traces from 3 of 7 PegAssist animals (PA2, PA5, and PA6) that developed spontaneous seizures after in utero prime editing with *Grin2a*-A243V. PA2 and PA5 developed frequent focal seizures, while PA6 presented a generalized seizure (EEG traces of both hemispheres shown) and sparse epileptiform events. Insets display magnifications of the indicated positions, showing spike-and-wave morphologies. Scale bars as indicated for full traces (top values) and insets (bottom values). (**B**) Morlet wavelet spectrograms of seizures in (a) showing characteristic dominant frequency bands and harmonics. Heatmap and scale bars = 10 s (PA2 and PA5) and 30 s (PA6). (**C**) Cumulative histogram of seizures over a 4-day recording period from PegAssist (PA; N=7) and control (CT; N=6) animals. Steps in cumulative histogram of PA cohort suggest circadian periodicity of seizures. (**D**) Seizures (solid circles) and epileptiform events (dashed circles) for each animal plotted by time and duration over 4-day recording period. Circle size indicates duration as indicated on the bottom right reference circles (10, 20, 40, 80, 160 s). Grey vertical bars indicate daily dark cycle. (**E**) Circadian histogram of seizures by hour in animal PA2 (dark blue) and PA5 (light blue). Seizures cluster in the 7:00-8:00 pm interval, corresponding to the beginning of the dark cycle when mice typically awaken.

Aggregating events within groups after blinded review of video and EEG recordings over 4 days, the PA cohort had a total of 107 seizures and an additional 56 epileptiform events, compared to 3 total events classified as seizures from one animal (CT3) electroporated with Cas9 and scrambled gRNA from the control cohort (Fig. 3C, fig. S5, and table S1). We anticipated that only a subset of PA animals would manifest phenotypes due to the known variability of electroporation between individually treated embryos. For the PegAssist workflow, we propose that the treated animal cohort be segmented into spontaneously symptomatic and non-symptomatic animals. Symptomatic animals would then be monitored to establish individual baseline seizure frequency as shown in Fig. 3D, and would then each constitute a personalized patient model for use in N-of-1 type testing of compounds to assess antiepileptic efficacy.

Within each animal, seizures were highly stereotyped, both behaviorally (movies S1-4) and electrographically (Fig. 3, fig. S5). Averaged traces of all events demonstrate that each animal's seizures displayed characteristic morphology and frequency (fig. S5), theoretically facilitating rapid automated analysis of seizure burden in subsequent N-of-1 trials. An interesting pattern also emerged when analyzing seizure event distribution. In the two animals with frequent seizures, events displayed clear circadian rhythmicity (Fig. 3C), with seizures clustering around lights-off (Fig. 3D), the time when mice typically transition to periods of wakefulness (*22*, *23*). This distribution mirrors a characteristic pattern in SeLECTs, wherein seizures most often occur during non-REM sleep or immediately after waking (*24*), further adding clinical validity as a patient model. Finally, the presence of frequent spontaneous seizures contributes to the model's utility in assessing patient-specific anti-seizure pharmacotherapy.

Potential for personalized medicine applications with PegAssist models

Our results provide initial evidence for the feasibility, validity, and utility of in utero genome editing to model an epilepsy patient variant in wildtype mice. The PegAssist approach holds several advantages over other modeling strategies: 1) The use of outbred wildtype animals diminishes cost and time of animal production, and increases genetic and behavioral robustness (*25*). 2) Since editing in each cell is a distinct event, rare off-target edits are not amplified and are unlikely to influence outcomes, avoiding clonal artifacts that afflict animal-lines (*26*). 3) The technology used is not species-limiting, meaning a similar approach can be used in non-rodent mammals, including non-human primates.

PE has been successfully applied to a variety of genomic loci in vitro and more recently in vivo (*27*, *28*), suggesting this approach is likely applicable to a wide range of genetic epilepsies. We propose that this pipeline may be a valuable tool for assessing personalized pharmacotherapy options for individual patients, and for preclinical assays for ultra-rare genetic disease in the drug development process.

References and Notes

1. S. T. Demarest, A. Brooks-Kayal, From molecules to medicines: the dawn of targeted therapies for genetic epilepsies. *Nat. Rev. Neurol.* **14**, 735–745 (2018).
2. J. K. Knowles *et al.*, Precision medicine for genetic epilepsy on the horizon: Recent advances, present challenges, and suggestions for continued progress. *Epilepsia*. **63**, 2461–2475 (2022).
3. Epi25 Collaborative, S. Chen, B. M. Neale, S. F. Berkovic, Shared and distinct ultra-rare genetic risk for diverse epilepsies: A whole-exome sequencing study of 54,423 individuals across multiple genetic ancestries. *medRxiv* (2023), doi:10.1101/2023.02.22.23286310.
4. P. Kwan, M. J. Brodie, Early identification of refractory epilepsy. *N. Engl. J. Med.* **342**, 314–319 (2000).
5. K. Saha *et al.*, The NIH Somatic Cell Genome Editing program. *Nature*. **592**, 195–204 (2021).
6. J. A. Doudna, The promise and challenge of therapeutic genome editing. *Nature*. **578**, 229–236 (2020).
7. A. V. Anzalone, L. W. Koblan, D. R. Liu, Genome editing with CRISPR-Cas nucleases, base editors, transposases and prime editors. *Nat. Biotechnol.* **38**, 824–844 (2020).
8. M. Charpentier *et al.*, CtIP fusion to Cas9 enhances transgene integration by homology-dependent repair. *Nat. Commun.* **9**, 1133 (2018).
9. A. V. Anzalone *et al.*, Search-and-replace genome editing without double-strand breaks or donor DNA. *Nature*. **576**, 149–157 (2019).
10. R. R. Richardson *et al.*, Enhancing Precision and Efficiency of Cas9-Mediated Knockin Through Combinatorial Fusions of DNA Repair Proteins. *The CRISPR Journal* (2023), doi:10.1089/crispr.2023.0036.
11. J. Y. Hsu *et al.*, PrimeDesign software for rapid and simplified design of prime editing guide RNAs. *Nat. Commun.* **12**, 1034 (2021).
12. G. Yu *et al.*, Prediction of efficiencies for diverse prime editing systems in multiple cell types. *Cell* (2023), doi:10.1016/j.cell.2023.03.034.
13. J. R. Lemke *et al.*, Mutations in GRIN2A cause idiopathic focal epilepsy with rolandic spikes. *Nat. Genet.* **45**, 1067–1072 (2013).
14. A. García-Recio *et al.*, GRIN database: A unified and manually curated repertoire of GRIN variants. *Hum. Mutat.* **42**, 8–18 (2021).
15. M. Salmi *et al.*, Impaired vocal communication, sleep-related discharges, and transient alteration of slow-wave sleep in developing mice lacking the GluN2A subunit of N-methyl-d-aspartate receptors. *Epilepsia*. **60**, 1424–1437 (2019).
16. V. Strehlow *et al.*, GRIN2A-related disorders: genotype and functional consequence predict phenotype. *Brain*. **142**, 80–92 (2019).
17. A. Amador *et al.*, Modelling and treating GRIN2A developmental and epileptic encephalopathy in mice. *Brain*. **143**, 2039–2057 (2020).
18. K. Robasky, N. E. Lewis, G. M. Church, The role of replicates for error mitigation in next-generation sequencing. *Nat. Rev. Genet.* **15**, 56–62 (2014).
19. P. Paoletti, P. Ascher, J. Neyton, High-affinity zinc inhibition of NMDA NR1-NR2A receptors. *J. Neurosci.* **17**, 5711–5725 (1997).

20. G. Gobbi, A. Boni, M. Filippini, The spectrum of idiopathic Rolandic epilepsy syndromes and idiopathic occipital epilepsies: from the benign to the disabling. *Epilepsia*. **47 Suppl 2**, 62–66 (2006).
21. M. Beaussart, Benign epilepsy of children with Rolandic (centro-temporal) paroxysmal foci. A clinical entity. Study of 221 cases. *Epilepsia*. **13**, 795–811 (1972).
22. B. Jin, T. Aung, Y. Geng, S. Wang, Epilepsy and its interaction with sleep and circadian rhythm. *Front. Neurol.* **11**, 327 (2020).
23. J. A. Ripperger, C. Jud, U. Albrecht, The daily rhythm of mice. *FEBS Lett.* **585**, 1384–1392 (2011).
24. N. Specchio *et al.*, International League Against Epilepsy classification and definition of epilepsy syndromes with onset in childhood: Position paper by the ILAE Task Force on Nosology and Definitions. *Epilepsia*. **63**, 1398–1442 (2022).
25. A. H. Tuttle, V. M. Philip, E. J. Chesler, J. S. Mogil, Comparing phenotypic variation between inbred and outbred mice. *Nat. Methods*. **15**, 994–996 (2018).
26. T. Doetschman, Influence of genetic background on genetically engineered mouse phenotypes. *Methods Mol. Biol.* **530**, 423–433 (2009).
27. S. Zhi *et al.*, Dual-AAV delivering split prime editor system for in vivo genome editing. *Mol. Ther.* **30**, 283–294 (2022).
28. J. R. Davis *et al.*, Efficient prime editing in mouse brain, liver and heart with dual AAVs. *Nat. Biotechnol.* (2023), doi:10.1038/s41587-023-01758-z.
29. C. D. Richardson, G. J. Ray, M. A. DeWitt, G. L. Curie, J. E. Corn, Enhancing homology-directed genome editing by catalytically active and inactive CRISPR-Cas9 using asymmetric donor DNA. *Nat. Biotechnol.* **34**, 339–344 (2016).
30. T. Saito, N. Nakatsuji, Efficient gene transfer into the embryonic mouse brain using in vivo electroporation. *Dev. Biol.* **240**, 237–246 (2001).
31. A. Poulopoulos *et al.*, Subcellular transcriptomes and proteomes of developing axon projections in the cerebral cortex. *Nature*. **565**, 356–360 (2019).
32. K. Clement *et al.*, CRISPResso2 provides accurate and rapid genome editing sequence analysis. *Nat. Biotechnol.* **37**, 224–226 (2019).
33. W. F. Borschel *et al.*, Gating reaction mechanism of neuronal NMDA receptors. *J. Neurophysiol.* **108**, 3105–3115 (2012).
34. S. A. Amico-Ruvio, S. E. Murthy, T. P. Smith, G. K. Popescu, Zinc effects on NMDA receptor gating kinetics. *Biophys. J.* **100**, 1910–1918 (2011).
35. D. L. Brody, P. G. Patil, J. G. Mulle, T. P. Snutch, D. T. Yue, Bursts of action potential waveforms relieve G-protein inhibition of recombinant P/Q-type Ca2+ channels in HEK 293 cells. *J. Physiol. (Lond.)*. **499 (Pt 3)**, 637–644 (1997).
36. L. J. Hirsch *et al.*, American clinical neurophysiology society's standardized critical care EEG terminology: 2021 version. *J Clin Neurophysiol*. **38**, 1–29 (2021).

Acknowledgments: We are grateful to Gabriela Popescu (Buffalo), Linda Nowak (Ithaca), and Cornelia Poulopoulou (Athens) for helpful discussions and technical advice. We thank Elise Caraker, Corinne Martin, Robert Lease (Baltimore), and Corey Flynn (Boston) for technical expertise. We are grateful for the technical and instrumentation support of the University of Maryland School of Medicine Center for Innovative Biomedical Resources through the Confocal Imaging Facility, the Flow Cytometry Facility, and the Institute for Genome Sciences Genomics Facility.

Funding:

National Institutes of Health grant DP2MH122398 (AP)

National Institutes of Health grant R01HL149926 (IED)

National Institutes of Health grant R37NS125632 (PBC)

UMSOM Training Program in Integrative Membrane Biology T32 fellowship (CDR)

UMSOM Training Grant in Cancer Biology T32 fellowship (RRR)

American Heart Association Postdoctoral Fellowship (DCOV)

Esther A. & Joseph Klingenstein Fund and the Simons Foundation Klingenstein-Simons Fellowship Award in Neurosciences (SBEW)

Author contributions:

Conceptualization: CDR, PD, AP

Methodology: CDR, PD, RRR, PHI, DCOV, MS, PNM, AJR, GC, EJ, SBEW, BNM, TLB, IED, AP

Investigation: CDR, PD, RRR, DCOV, IED, AP

Visualization: CDR, PD, DCOV, IED, AP

Funding acquisition: PBC, SBEW, IED, AP

Project administration: AP

Supervision: BNM, TLB, PBC, IED, AP

Writing – original draft: CDR, PD, AP

Writing – review & editing: all authors

Supplementary Materials

Materials and Methods

Figs. S1 to S5

Table S1 to S2 descriptions

Movie S1-S4 descriptions

Supplementary Materials for

Modeling an ultra-rare epilepsy variant in wildtype mice with in utero prime editing

Colin D. Robertson[1], Patrick Davis[2], Ryan R. Richardson[1], Philip H. Iffland II[3], Daiana C. O. Vieira[4], Marilyn Steyert[1]†, Paige N. McKeon[1], Andrea J. Romanowski[1], Garrett Crutcher[1], Eldin Jašarević[1]†, Steffen B. E. Wolff[1], Brian N. Mathur[1], Peter B. Crino[3], Tracy L. Bale[1]†, Ivy E. Dick[4], Alexandros Poulopoulos[1]*

[1]Department of Pharmacology and UM-MIND, University of Maryland School of Medicine, Baltimore, MD, USA

[2]Department of Neurology, Boston Children's Hospital, Harvard Medical School, Boston, MA, USA

[3]Department of Neurology, and UM-MIND, University of Maryland School of Medicine, Baltimore, MD, USA

[4]Department of Physiology and UM-MIND, University of Maryland School of Medicine, Baltimore, MD, USA

*Corresponding author. Email: apoulopoulos@som.umaryland.edu

†Current affiliations: MS: Department of Neurological Surgery, University of California San Francisco; EJ: Department Computational and Systems Biology, Department of Obstetrics, Gynecology and Reproductive Sciences, University of Pittsburgh School of Medicine; TB: Department of Psychiatry, University of Colorado School of Medicine.

Materials included:

Materials and Methods
Figs. S1 to S5
Table S1 to S2 descriptions
Movie S1-S4 descriptions

Materials and Methods

pegRNA design and PegAssist application

To facilitate the use and broad adoption of prime editing, we developed PegAssist and an accompanying webtool and set of plasmids for the design and production of custom Prime editing reagents. The python-based web application pegassist.app accepts input of target sequence and desired edits to produce pegRNA sequences and one-step cloning strategies based on the PegAssist plasmid set. The PegAssist platform offers PE2, PE3 and PE3b variant strategies, and further allows custom modifications of spacers and PAM sequences for versatility and use with further developments in genome editors (fig. S2).

The PegAssist python source code is available on github.com/pegassist. A graphical user interface was created using Heroku to compile a webtool available at pegassist.app.

To generate *Grin2a*-A243V pegRNAs, a custom spacer (20 nt) was first designed to minimize the distance between the protospacer adjacent motif (PAM) site and the edit position. The custom spacer and desired edit were used to generate automated reverse transcriptase template and primer binding sequence options and secondary nicking (PE3/PE3b) guides following the instructions outlined by the webtool. Preference was given to PBS ~13nt with >30% GC-content and RT <20nt. PE3b guides were selected to minimize unintended indels.

Plasmids

Double-stranded DNA oligonucleotides containing pegRNAs flanked by BbsI recognition sites were synthesized by Twist Bioscience. Sense and antisense oligonucleotides for knockout gRNA or PE3b gRNA with overhangs for golden gate assembly were synthesized by Integrated Design Technologies. Cloning was performed as previously described (*10*). Briefly, pegRNA oligonucleotides were sub-cloned into pCR Blunt II-TOPO backbone (ThermoFisher). A golden gate assembly (GGA) with BbsI was used to clone the pegRNA into a custom backbone containing a hU6 promotor. The PE3/PE3b or knockout gRNA sense and antisense oligonucleotides were annealed and cloned by GGA into a pJ2 (*10*) containing a hU6 promoter. The vectors containing pegRNA and PE3/PE3b guides were used as template for PCR using KAPA HiFi HotStart DNA Polymerase with 2x Master Mix (Roche) to amplify parts containing the U6 promoter and either the pegRNA or PE3/PE3b guide using primers with BsaI recognition sites. These parts were assembled in a final vector by golden gate assembly using NEB Golden Gate Assembly Kit according to manufacturer's recommendations. The open reading frame of PE2 was extracted from pCMV-PE2 (Addgene plasmid #132775) by PCR with primers (prRR842 and prRR849). PE2 was introduced into a pJ2 backbone by GGA to construct the final plasmid pJ2.CAG<EGFP-2A-PE2 [Lab plasmid ID: TU516]. Plasmid pCAG<myr-tdTomato expressing myristoylated tdTomato was subcloned from Addgene plasmid #26771 and used as a bright fluorescence electroporation reporter. Plasmid sequences were confirmed by Sanger sequencing by GeneWiz. Details and sequences of plasmids and oligonucleotides used are listed in table S2.

BFP-to-GFP conversion assay

BFP-to-GFP conversion assays were performed as previously described (*10*). Briefly, a modified HEK-293 cell line with genomically-encoded BFP was a gift from the Corn lab (*29*). Cells were maintained in DMEM with GlutaMAX (ThermoFisher Scientific) supplemented with 10% fetal bovine serum. Cells were plated at a density of 20,000-22,500 cells/cm^2 in 24-well plates prior to transfection using polyethylenimine, linear, MW 25000 (Polysciences) at 1 mg/mL in diH_2O, then mixed in a 3:1 ratio with 750 ng total DNA diluted in Opti-MEM per well.

Conversion of BFP to GFP was analyzed by flow cytometry using an LSRII cell analyzer with HRS (BD Biosciences). A 407 nm laser with a 405/50 emission filter was used to detect BFP, while a 488 nm laser with a 505 LP mirror and a 530/30 emission filter was used to measure GFP.

Mice

Experimental protocols involving animals were approved by the University of Maryland Baltimore Institutional Animal Care and Use Committee. Pregnant, outbred CD1 mice were obtained from Charles River Laboratories. *In utero* electroporation was performed on embryonic mice ambiguous to considerations of sex. Mice were weaned at P21 and EEG/EMG recordings were performed at 3-8 months.

In utero electroporation

Cortical layer II/III pyramidal neurons were targeted by performing this procedure *in utero* on embryonic day 14.5 as previously described (*30*, *31*). Briefly, plasmid DNA was combined to a maximum concentration of 4 µg/µL with equal molar ratios of relevant plasmids (pegRNA/ PE3b duplex, prime editor, and fluorescent reporter). Dams were anesthetized with isoflurane with thermal support. The abdomen was prepared for surgery by removing hair and sanitizing the incision site using betadine and 70% ethanol. An incision of the skin and muscle layer along the midline exposed the uterine horns. A glass micropipette was pulled (Narishige PC-100) and beveled (Narishige PCR-45). The micropipette was attached to an aspirator and used to inject the prepared DNA mixture into the right ventricle of developing fetuses. Immediately upon injection, a series of 4 x 50 ms square pulses of 35 V (NEPA21 electro-kinetic platinum tweezertrodes on a BTX ECM-830 electroporator) was used to introduce the DNA into neural progenitor cells lining the ventricle. In a typical surgery 3-6 pups were electroporated. Following electroporation, the uterine horn was returned to the abdominal cavity, and the muscle and skin layers were closed using monofilament nylon sutures (AngioTech). After birth, electroporated pups were screened at post-natal day 0 for fluorescence using a fluorescence stereoscope (Leica MZ10f with X-Cite Fire LED light source). Positively screened pups were returned to the dam.

Neuron Fluorescence Activated Cell Sorting and Next-Generation Sequencing

In utero electroporated mice were deeply anesthetized using isofluorane and euthanized. The brain was removed and immediately moved to pre-cooled dissociation medium (20 mM glucose, 0.8 mM kynurenic acid, 0.05 mM APV, 50 U/ml penicillin, 0.05 mg/mL streptomycin, 0.09 M Na_2SO_4, 0.03 M K_2SO_4, 0.014 M $MgCl_2$) on ice. Using a fluorescence stereoscope (Leica MZ10f with X-Cite Fire LED light source), the electroporated region was dissected and transferred to a new tube containing ice-cold dissociation medium. Dissociation medium was

aspirated until 1 mL remained and an activated papain solution (1:1 papain [Worthington-Biochem] with 13.6 mM Cysteine-HCL, 0.002% β-mercaptoethanol, and 2.4 mM EDTA pH 8.0 in MilliQ water) was added and incubated at 37° C for 30 minutes. Papain solution was removed, and tissue was washed three times and resuspended in 500 µL fresh dissociation medium. Samples were triturated 2-4 times using flame-polished borosilicate pipettes. Cell suspensions were sorted at low flow rates using a Wolf Benchtop Cell Sorter (Nanocollect Biomedical, Inc.) using red fluorescence from pCAG<myr-tdTomato for gating, after confirming overlap with green fluorescent signal from co-expressed pJ2.CAG<EGFP-2A-PE2. Approximately 3,000 cells were collected per sample. Sorted cells were pelleted and stored at -80°C.

Cells were lysed and total RNA was extracted using an AllPrep DNA/RNA Micro Kit (Qiagen). A reverse transcription reaction using a First Strand cDNA Synthesis Kit (Millipore Sigma) was used to create cDNA from the isolated RNA. The region surrounding the intended edit was amplified by PCR using primers containing universal adaptor sequences (prCR419 and prCR420). These amplicons were submitted to the Institute for Genome Sciences at the University of Maryland School of Medicine for sequencing, where samples were quantified, barcoded and sequenced on an Illumina NextSeq 550 (Illumina) according to manufacturer settings. An average of 8.9 million reads per sample were analyzed. GRCm39 was used as reference genome. Sanger sequencing of the target region from CD1 mice used in experiments were consistent with the reference genome (data not shown). Sequencing results were analyzed using CRISPResso2 (*32*) under prime editing mode. Default CRISPResso2 parameters were applied (quantification window 10, nicking guide sequence defined, scaffold match length 1). A contiguous quantification window was produced encompassing both pegRNA and PE3b gRNA target sequences.

Electrophysiology

Whole-cell currents were recorded at room temperature from mouse cortical neurons which were isolated at P0 from E15 in utero electroporated animals and cultured 30 days in vitro (DIV) in order to allow for expression of GluN2A, which is known to be developmentally regulated (*33*). Only cells expressing the red fluorescent marker were patched. Electrodes were pulled from borosilicate glass capillaries that were fire-polished to a resistance of 3-4 MΩ and filled with intracellular solution (mM): 135 CsCl, 35 CsOH, 4 MgATP, 0.3 Na_2GTP, 10 HEPES and 1 EGTA, adjusted to pH 7.4 with CsOH. Cells were perfused with extracellular solutions containing (mM): 140 NaCl, 2.5 KCl, 1.8 $CaCl_2$, 0.1 glycine, 10 HEPBS, 10 tricine, adjusted to pH 7.4 (NaOH). 40 µM cyanquixaline (CNQX) and 1µM ifenprodil were added to external solution to block GluN2B and AMPA receptors respectively. For solutions containing zinc, free Zn^{2+} concentrations in 10 mM tricine-buffered solutions were calculated using Maxchelator software (Chris Patton) using a binding constant of 10^{-5} M as previously reported (*19*) and adjusted for our conditions. The final free zinc concentration was chelated to 67 nM by adding 200 mM $ZnCl_2$ and 10 mM tricine into the working extracellular solution (*34*). Currents were recorded with an Axopatch 200B amplifier (Molecular Devices) and digitized using an iTC-18 (InstruTECH). Currents were low-pass filtered at 2 kHz and sampled at 10 kHz using custom MATLAB (MathWorks) scripts. Drugs and agonists were applied during the patch recordings by means of an eight-barrel pen-perfusion system, with minimal dead space. In all whole-cell

experiments, the cells were clamped at -80 mV. Solution containing NMDA (100 μM), or NMDA with 67 nM free Zn^{2+} was applied to elicit the current, usually for 5 sec every 2 min, using motor-driven valves.

For HEK 293 cell recordings, cells were cultured on glass coverslips coated with poly-D-lysine and transfected via the calcium phosphate method (*35*) with 4–8 μg of rat GluN1-1a and GluN2A or GluN2A (A243V), and co-transfected with 2 μg green fluorescent protein. Culture media was exchanged 3–5 h post-transfection, and cells were maintained 24–48 hours in DMEM supplemented with 2 mM Mg^{2+} to prevent NMDA receptor-mediated cell death. The GluN1-1a and GluN2A plasmids were a kind gift from Gabriela Popescu (University at Buffalo). The mutation A243V was introduced into the GluN2A plasmid using the QuickChange II XL kit from Agilent. All portions of the resulting construct that were subject to PCR were confirmed by DNA sequencing. Recording conditions were identical to those listed above for neurons.

Continuous EEG/EMG recording

Synchronous EEG/EMG and video recording was performed using a tethered, 3-channel recording system from Pinnacle Technology Inc. Prefabricated EEG headmounts were implanted with screw electrodes 3 mm behind Bregma and an EMG lead was implanted in the trapezius muscle of mice under isofluorane anesthesia. Mounted electrodes were fixed using dental epoxy. After minimum 72 hours recovery, mice were placed in recording chambers for synchronous EEG/EMG and video recording for approximately 4 days.

The EEG/EMG data were exported and blinded before primary review. An initial investigator manually annotated possible epileptiform events and exported epochs for secondary review by a blinded expert (author PFD) and classification based on the American Clinical Neurophysiology Society's most recent standardized criteria (*36*). Specifically, seizure was defined as any rhythmic epileptiform discharge with either a) time-locked, consistent behavioral correlate, b) discharges averaging >2.5Hz for at least 10s, or c) with definite spatiotemporal evolution and lasting at least 10s. Based on accepted ACNS criteria for human EEG, the latter two categories would be termed "electrographic seizure" as opposed to "electroclinical seizure", but in this analysis we did not make such a distinction.

EEG, EMG, and video data were used to visually identify artifacts associated with movement. If movement associated with EEG change was stereotyped across events (within animals) (see videos S1-4), the abnormal movements associated with these events were considered clinical correlates. Seizure events were further classified as lateralized for events occurring in only one EEG channel or generalized for events with synchronous activity between both EEG channels. If similar activity was seen that was without clear clinical correlate, did not last 10s duration, and did not have clear spatiotemporal evolution, these events were classified as interictal discharges ("epileptiform" in table S1 and fig. S5) as opposed to seizures. Seizure epoch charts were generated from annotated seizure bouts using MNE-Python following standardization using the SciKit StandardScaler function. Seizure frequency was calculated as the total number of events divided by days of recording.

Tissue Fixation and Immunolabeling

Tissue was fixed by transcardial perfusion of mice using PBS and 4% paraformaldehyde with 24 hours post-fixation in 4% paraformaldehyde at 4°C. Tissue slices were cut to 80 µm using a vibrating microtome (Leica). For immunolabeling, slices were incubated in a blocking solution of 5% BSA, 0.3% TritonX-100, and 0.05% sodium azide in PBS for 2 hours while rocking at room temperature. Primary antibodies were diluted 1:1000 in blocking solution, and tissue was incubated overnight, rocking at room temperature. Slices were washed 3x 30 minutes in PBS while rocking, then incubated with secondary antibody at 1:1000 in PBS at room temperature for 4 hours. After 3x 30-minute PBS washes the slices were mounted on slides with either Fluoromount-G Mounting Medium with or without DAPI (ThermoFisher Scientific).

Microscopy

Fluorescence images were acquired using a Nikon Ti2-E inverted epifluorescence microscope. Images were analyzed using NIS Elements (Nikon). Proximal z-stacks were acquired using a 10x objective, then extended depth of focus and stitching were used to compile a single slice image.

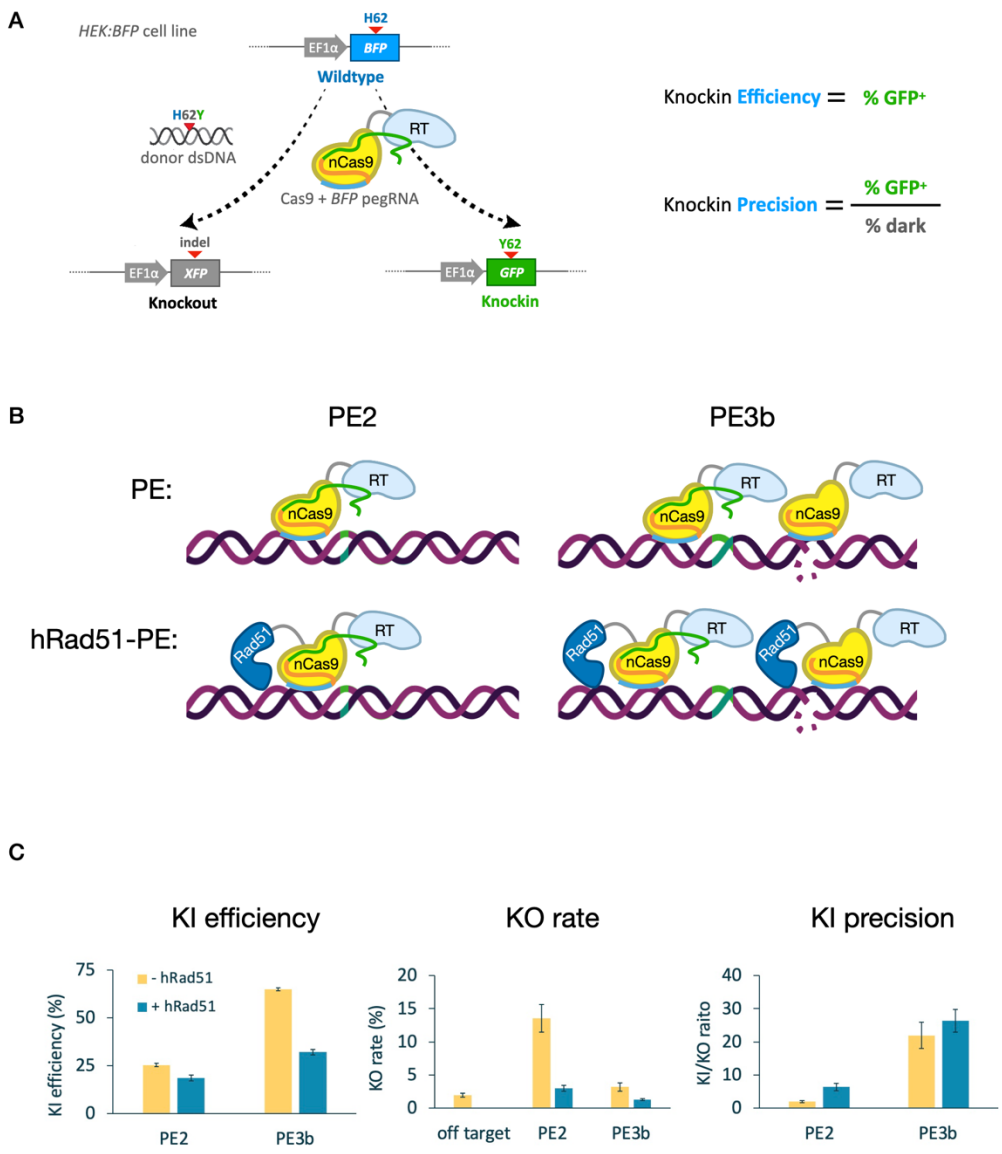

Fig. S1.

Screening editing agents for precision identifies prime editing with PE3b as highest precision for point editing. (**A**) Schematic (adapted[10]) depicting the BFP-to-GFP conversion assay. HEK cells with genomic knockin of BFP were transfected with editing agents to introduce H62Y edit, which corresponds to the sequence of GFP. Precise editing converts cells from blue to green, while imprecise edits cause loss of fluorescence. Editing precision is calculated as the ratio of green/dark cells. (**B**) Schematic of the editing approaches tested with the assay. Standard PE2 and PE3b approaches were tested in combination with an hRad51-fused prime editor. (**C**) Quantification of knockin efficiency, knockout rate, and knockin precision. Addition of hRad51 improved PE2 strategy's precision but did not significantly improve PE3b. The standard PE3b approach provided the highest efficiency and precision.

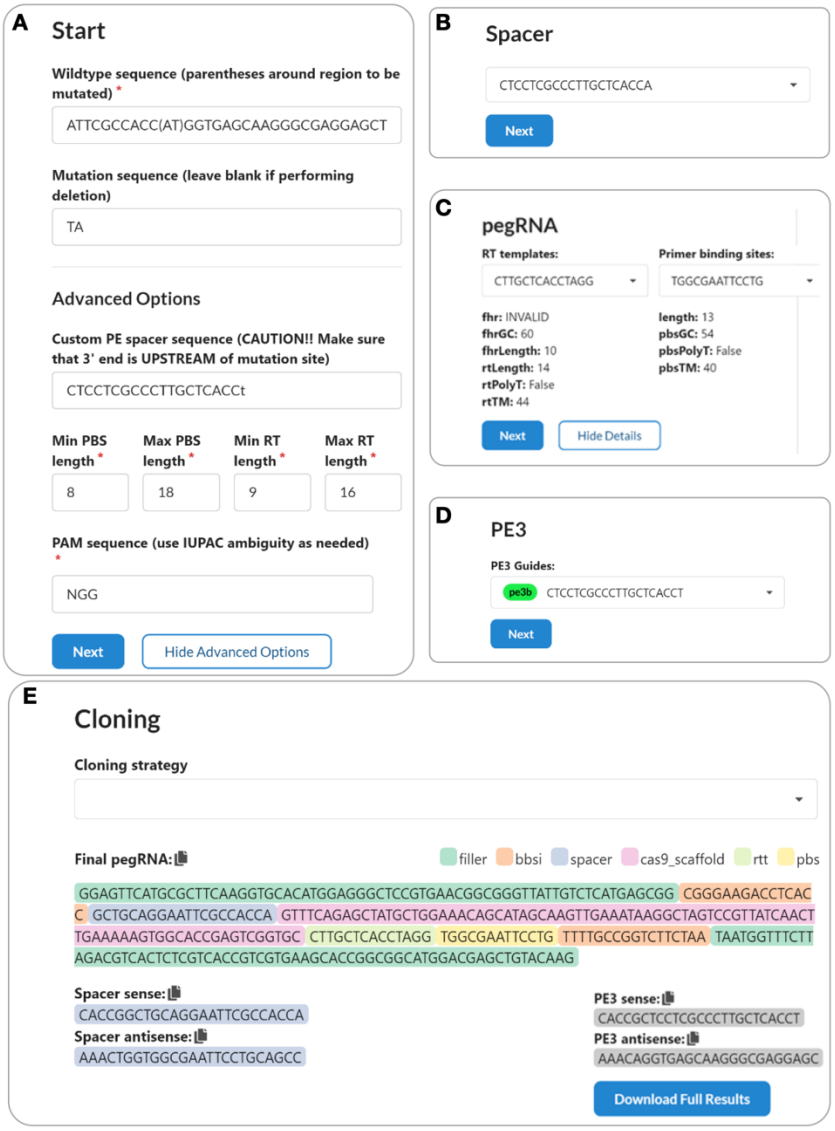

Fig. S2.

pegassist.app simplifies pegRNA and PE3b guide design. (**A**) pegassist.app accepts input of a wildtype sequence with the desired edit in parentheses. The edited sequence is entered, and users can select from additional options including input of a pre-designed spacer sequence. (**B**) A spacer sequence is selected from the dropdown menu. (**C**) RT template and Primer binding site options are presented with warnings against low efficiency. (**D**) All PE3/PE3b options are presented for selection. (**E**) pegassist.app displays a final pegRNA and the required oligos based on the selected cloning method.

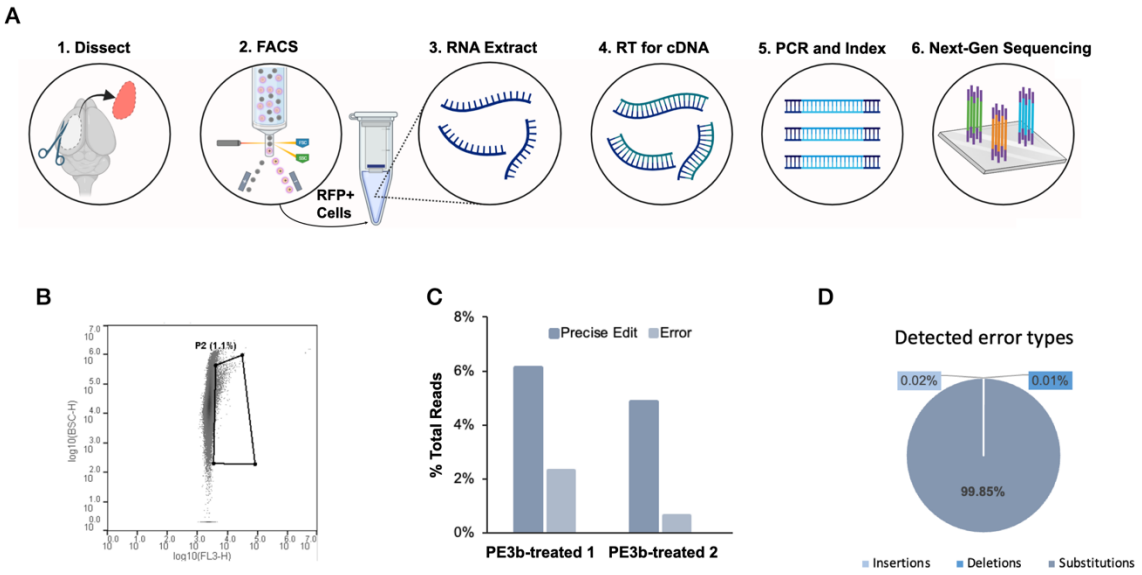

Fig. S3.

In vivo prime editing of *Grin2a* is precise and causes few indels. (**A**) Schematic representation of the sequencing workflow. Following in utero electroporation with PE3b agents, the PE-expressing region of cortex was dissected from adult mice. Cells were triturated and sorted for red fluorescence. RNA was extracted to generate cDNA by reverse transcription. Target sequence was amplified by PCR. Amplicons were indexed and sequenced on the Illumina NextSeq platform. (**B**) FACS plot of neurons gated to collect electroporated red fluorescent neurons (~1% of total neurons). y axis plots side scatter and x axis plots red fluorescence intensity. (**C**) Percentage of reads with either the intended edit or any error in the two PE3b-treated animals sequenced. The intended edit is detected approximately 5 times more frequently than the aggregate of all proximal erroneous edits. (**D**) Breakdown of error types detected in PE3b-treated samples. Most errors are substitutions and may be expected to have less deleterious effects on the resulting protein than indels.

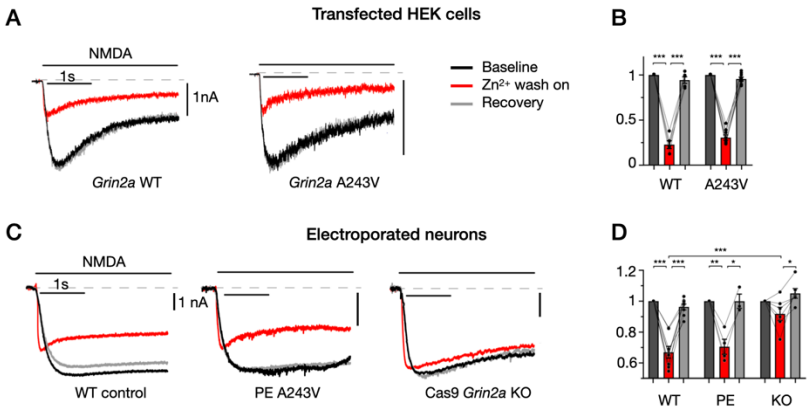

Fig. S4.

Electrophysiology shows *Grin2a* KO is not a common outcome of in utero PE3b. (**A**) Example traces (black=baseline, red=zinc wash-on, grey=recovery) and (**B**) normalized (within sample to baseline) amplitudes of currents recorded from HEK cells co-transfected with *GRIN1* and either WT (n=5) or A243V (n=8) variant of *GRIN2A*. No change in the sensitivity to Zn2+ blockade of NMDA currents. (**C**) Example traces and (**D**) normalized (within sample to baseline) amplitudes of currents recorded from in utero electroporated neurons after cultured after in utero electroporation. Zinc blockade was detected in Sham (n=8) and PE *Grin2a-A243V* cells (n=4), but not KO cells (n=6), indicating that treatment with PE3b does not cause significant loss-of-function (*p<0.05, ***p<0.001, via students T-test).

Fig. S5

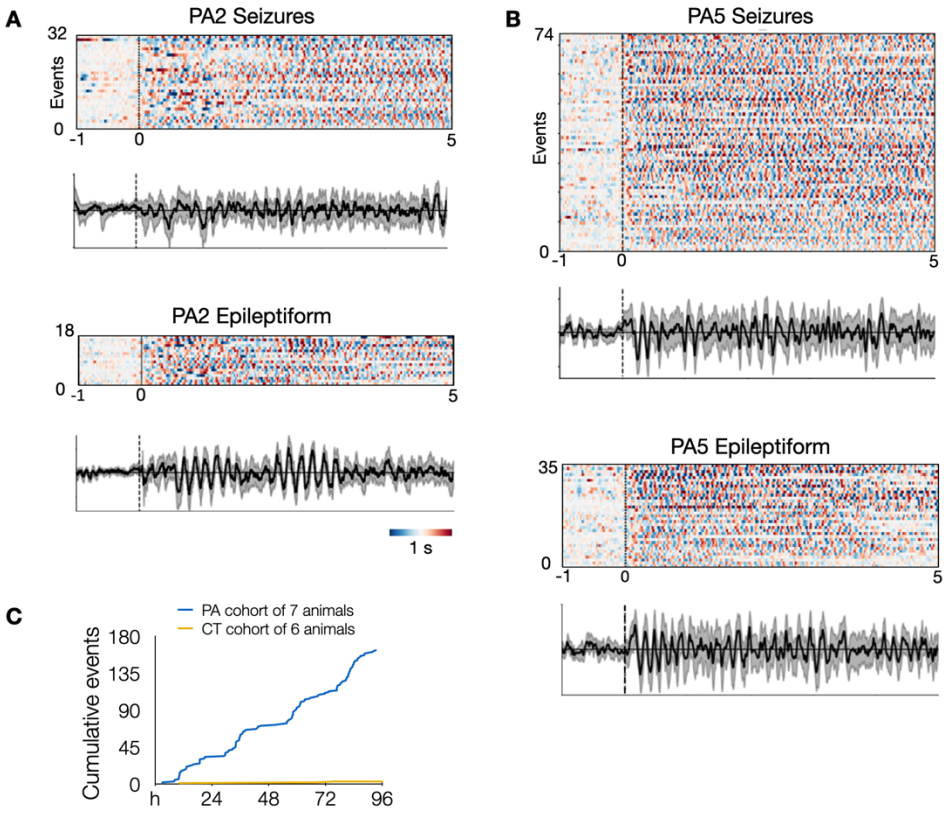

Fig. S5.

Epoch charts and averaged traces show the stereotyped nature of seizures and epileptiform events. (**A**) PA2 and (**B**) PA5 epoch charts and averaged traces for events classified as seizures or epileptiform events. Each row represents a separate event aligned at onset of abnormal activity (t = 0) and plotted from t = -1 s to t = 5 s. Color bar indicates standardized EEG amplitude from peak negative (dark blue) to peak positive (dark red). Traces show an averaged EEG signal in black with bootstrapped 95% confidence intervals in grey. Charts were generated using MNE-Python. (**C**) Pooled cumulative events (including both seizures and epileptiform events) between PA and CT groups over 4 days of EEG recording. Heatmap and scale bar = 1 s.

Table S1.

Individual annotation of seizures and epileptiform events ("Events" tab), and details of PA and CT animal cohorts ("Cohorts" tab).

Table S2.

Plasmids and oligonucleotides used: identifiers, purpose, and sequences.

Movie S1.

Videos of seizures corresponding to the first example trace from animal PA2 in Fig. 2A.

Movie S2.

Videos of seizures corresponding to the second example trace from animal PA2 in Fig. 2A.

Movie S3.

Videos of seizures corresponding to the first example trace from animal PA5 in Fig. 2A.

Movie S4.

Videos of seizures corresponding to the second example trace from animal PA5 in Fig. 2A.